JMEPEG (2015) 24:4863–4869
DOI: 10.1007/s11665-015-1782-9

1059-9495/$19.00

Oxidation Behavior of $Zr_{43}Cu_{45}Al_{12}$ Bulk Metallic Glass at 400-525 °C in Air Atmosphere

J. Dąbrowa, L. Perriere, M. Stygar, W. Kucza, Ł. Klita, and M. Danielewski

(Submitted August 9, 2015; in revised form September 28, 2015; published online November 2, 2015)

The oxidation behavior of $Zr_{43}Cu_{45}Al_{12}$ bulk metallic glass was studied over the temperature range 400-525 °C in air atmosphere. The oxidation kinetics of the material changes significantly, from the parabolic one in 400 °C to logarithmic kinetics in $T = 450$ °C and higher. The inversion of oxidation kinetics was observed. Composition of the scale varied over the examined temperature range, consisting mostly of monoclinic ZrO_2, tetragonal ZrO_2 and CuO, with minor amounts of α-Al_2O_3 within whole temperature range and Cu_2O in temperatures 400 and 450 °C. The α-Al_2O_3 presence can be correlated with decrease of oxidation rate in the higher temperatures.

Keywords corrosion, metallic glasses, oxidation, rapid solidification

1. Introduction

Since the advent of bulk metallic glasses (BMG), they have been intensively studied due to their unique properties, both mechanical and chemical. As bulk materials they can be used as structural materials, what makes deliberate studies on their behavior in elevated temperatures from the point of view of their future applications. One of the most extensively researched group of BMG are Zr-Cu-based glasses (Ref 1-5), which exhibits good glass forming ability (GFA) (Ref 6-8) and exceptional mechanical properties, such as high yield strength and strain (Ref 9-11). Oxidation behavior of Zr-based metallic glasses has been examined by several authors (Ref 12-15). Especially interesting results have been obtained for the Zr-Cu-Al ternary alloys (Ref 16-18) in which the inversion of oxidation kinetics is observed, as well as strong dependence of the scale composition on the temperature. Kai et al. (Ref 17, 18) reported a non-intuitive dependence of Al_2O_3 formation process on the concentration of Al in the alloy. For examined compositions of $Zr_{47.5}Cu_{47.5}Al_5$ and $Zr_{50}Cu_{43}Al_7$, the presence of α-Al_2O_3 phase was detected in much wider temperature range for the alloy with lesser Al content. It should also be noted that for the $Zr_{47.5}Cu_{47.5}Al_5$ alloy a tendency toward forming a ZrCu crystalline phase has been observed, while for $Zr_{50}Cu_{43}Al_7$, despite higher content of Zr in respect to Cu, a formation of $Cu_{10}Zr_7$ phase has been reported.

The main goal of this study was to investigate oxidation behavior of an amorphous alloy with relatively high Al content, $Zr_{43}Cu_{45}Al_{12}$, to expand the knowledge on the oxidation processes in BMGs from Zr-Cu-Al ternary system and especially on the Al role in the process. Most of the studies on the oxidation behavior of Zr-Cu-Al-based amorphous alloys is concentrated on the materials with low Al content (8 at.% or lower), what is probably dictated by the favorable glass forming abilities of these compositions (Ref 3). However, complexity of the mentioned processes suggest, that further studies on the scale formation on Zr-Cu-Al metallic glasses, which would cover alloys with Al content higher than 10 at.% are needed. A higher Al content in this case should promote formation of the Al_2O_3 protective scale and lead to a different (probably more favorable) oxidation behavior compared to already studied BMGs.

J. Dąbrowa, M. Stygar, W. Kucza, Ł. Klita, and **M. Danielewski**, Faculty of Materials Science and Ceramics, AGH University of Science and Technology, al. Mickiewicza 30, 30-059 Kraków, Poland; and **L. Perriere,** Institut de Chimie et des Matériaux Paris-Est (ICMPE), UMR 7182, CNRS & Université Paris-Est Créteil, 2-8 rue Henri Dunant, 94320 Thiais, France. Contact e-mails: dabrowa@agh.edu.pl and stygar@agh.edu.pl.

2. Materials and Methods

The $Zr_{43}Cu_{45}Al_{12}$ BMG was obtained by a twin-roll casting method described elsewhere (Ref 19). The ejection temperature during procedure was 1360 °C and melted alloy was ejected on the CuCoBe wheels under pressure of 150 mbar. As a result, an amorphous material in a form of a 380 μm thick sheet (approximately 2 cm wide, 20 cm long) was obtained. Samples used during oxidation experiments were cut with wire cutter into the 8 mm × 15 mm plates. Obtained samples were then polished on a Struers TegraPol-11 polishing machine, using standard Struers procedure. Thermal stability of the material was examined by differential-scanning calorimetry (DSC), using NETSZCH Pegasus 404 F1 DSC apparatus equipped with a thorium furnace. Thermal cycle was carried out from 40 up to 1000 °C and down, using a 20 °C/min heating and cooling rate. A protective flow of Ar, as well as zirconium getter were used to avoid oxidation of the samples. Oxidation tests were carried out using CI Electronics MK2-M5 balance head in air atmosphere. The samples were put into already heated TGA furnace, and hold in the given temperature for 12 h. The furnace was then free-cooled, to avoid problems with thermal stresses and spallation, reported by Kai et al. (Ref 17, 18). Characterization of the substrate and obtained scale was performed using x-ray diffraction (XRD) and scanning electron microscope (SEM) equipped with the x-ray energy-dispersive spectrometry (EDS).

3. Results and Discussion

3.1 Alloy Characterization

XRD spectra of the as-cast $Zr_{43}Cu_{45}Al_{12}$ shown in Fig. 1(a), revealed the presence of one wide-broadening peak typical for the amorphous phase. The composition was examined by quantitative ICP (Varian Vista Axial). Dissolution of the alloy was carried out in a HNO_3/HCl mixture (ratio of 2:3) at 110 °C for 3 h. Solutions were then diluted 10 times for the analyses. Obtained average composition in atomic percentages was as follows: 43.21% Zr, 45.30% Cu, and 11.50% Al. DSC curve of the examined alloy is presented in Fig. 1(b), the obtained T_g and T_x temperatures were 448.7 and 497 °C, respectively. The supercooled region (ΔT_x) was about 48.7 °C, what is slightly lower value than those reported for the $Zr_{47.5}Cu_{47.5}Al_5$ and $Zr_{50}Cu_{43}Al_7$ glasses (Ref 17, 18). It should also be noted, that the value of T_g equal to 497 °C is also comparatively higher.

3.2 Oxidation Kinetics

Oxidation kinetics plots are presented in Fig. 2. Obtained results are significantly different from those reported for $Zr_{47.5}Cu_{47.5}Al_5$ and $Zr_{50}Cu_{43}Al_7$ BMGs, as well as from other Zr-Cu-Al-based glasses, including those with a relatively high Al content, where multi-stage parabolic kinetics were reported (Ref 12, 16, 20, 21). In all measured cases, inversion of kinetics was observed, meaning that increase in temperature of the oxidation process led to decrease of mass gain per unit area.

At 400 °C (below T_g), a multi-stage kinetics was observed. Firstly, linear stage was observed for 20 min. The second stage takes time from 20 min to 2 h, in which interval the kinetics follow the parabolic law ($R^2 = 0.999$) with the k_p equal to 8.83×10^{-11} g^2/cm^4/s. The third stage can also be described by the parabolic law ($R^2 = 0.989$) with the k_p equal to 2.82×10^{-11} g^2/cm^4/s. These results are different from those obtained for $Zr_{50}Cu_{43}Al_7$ BMG, where two-stage kinetic was reported (Ref 18). Also, the mass gain per unit surface after 12 h was about 63% of that measured for $Zr_{50}Cu_{43}Al_7$.

At 450 °C (just after the onset of T_g) the material exhibits completely different kinetics, what may suggest formation of a new phase, which has a significant influence on mass transport processes. Two stages can be distinguished. The first one, up to 10 min, can be described by the linear law. The second stage follows the logarithmic (Ref 22):

$$\frac{\Delta m}{S} = k_1 \log(k_2 t + k_3), \qquad \text{(Eq 1)}$$

where Δm is the mass gain and S is the total area of oxidized sample. The determined values of k_1, k_2, and k_3 (obtained through optimization performed by conjugate gradient method) are presented in the Table 1 together with results obtained for higher temperatures. Similarly to the previous case, these results are different from those obtained for $Zr_{50}Cu_{43}Al_7$ BMG, where three-stage parabolic kinetic of oxidation was observed (Ref 18). In this temperature, the most significant difference in mass gain in comparison to the $Zr_{50}Cu_{43}Al_7$ can be observed, with the mass gain per unit surface being just 26% of that reported for the mentioned case.

At 500 °C (slightly higher than T_x), the material exhibits slightly different oxidation behaviors even though a two-stage kinetic is also observed. The first 5 min can be described by the linear law while the second stage can be fitted with the logarithmic function (although inverse logarithmic law also gives good agreement in this particular case). The total mass gain per unit surface was about 86% of that reported for $Zr_{50}Cu_{43}Al_7$ (Ref 18) with the difference being much less pronounced then in the case of 450 °C.

At 525 °C (after the first peak of crystallization), a linear stage can be observed during the first 5 min and logarithmic stage after this time.

Since the values of constants for logarithmic law are rather difficult to compare with the literature data, additional fittings for non-linear parts of kinetics with usage of parabolic law were performed based on the equation:

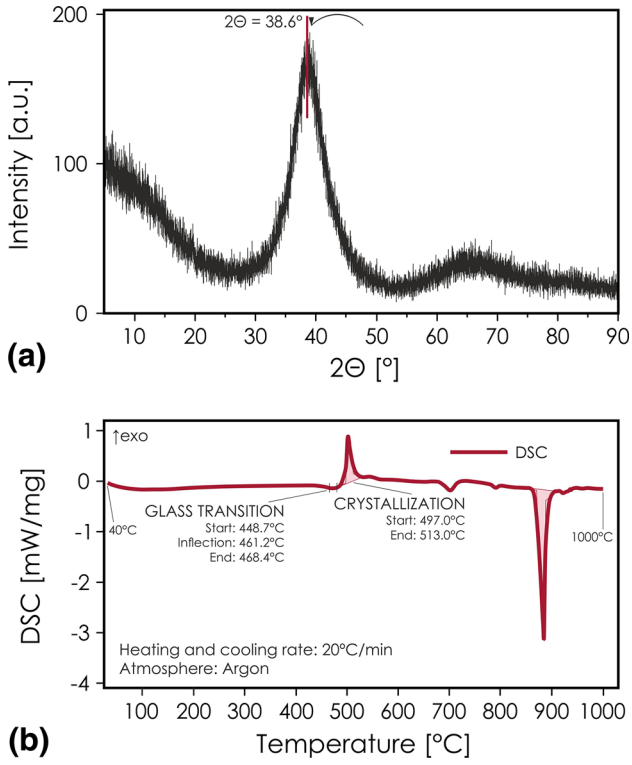

Fig. 1 XRD spectra (a) and DSC curve (b) of the $Zr_{43}Cu_{45}Al_{12}$ BMG obtained by twin-roll casting method

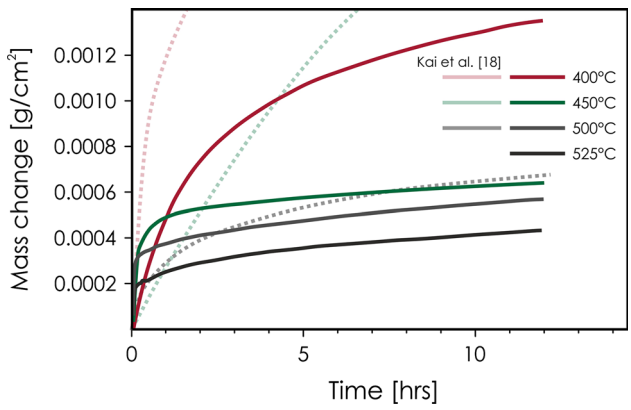

Fig. 2 Oxidation kinetics of $Zr_{43}Cu_{45}Al_{12}$ BMG. The values for $Zr_{43}Cu_{50}Al_7$ alloy [18] are given for comparison (Color figure online)

Table 1 Values of oxidation laws constants obtained for both logarithmic and parabolic fittings

	Logarithmic fit				Parabolic fit	
Temperature, °C	k_1	k_2	k_3	NRMSE (%)	k_p	NRMSE, %
400	...	...	...	...	1.41×10^{-11}(a)	0.78
450	6.47×10^{-5}	0.419	1.127	1.13	2.42×10^{-12}	3.67
500	7.53×10^{-5}	0.032	24.600	2.08	2.41×10^{-12}	2.11
525	9.44×10^{-5}	0.002	6.376	0.88	1.59×10^{-12}	3.29

The values of normalized root mean square errors (NRMSE) are given for comparison of the fittings quality
(a) For oxidation times higher than 2 h

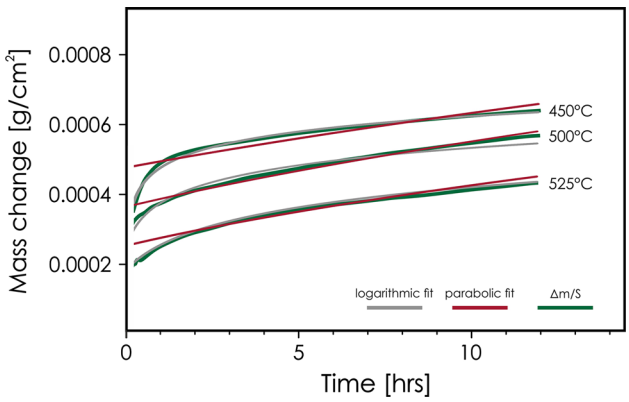

Fig. 3 Results of the fittings for both parabolic and logarithmic oxidation law assumed (Color figure online)

$$\left(\frac{\Delta m}{S}\right)^2 = 2k_p t + C. \quad \text{(Eq 2)}$$

As it can be seen in Fig. 3, the quality of such fittings is much lower than in the case of logarithmic ones. To show the quantitative difference between them, the normalized root mean square errors (NRMSE) were calculated for both types of fittings. The results together with values of fitted k_p are also presented in the Table 1. The biggest error in terms of the NRMSE for logarithmic fitting is observed for the case of kinetics recorded in 500 °C, in which the inverse logarithmic law could also be fitted. It should be noted, that fitted values of parabolic constants due to the logarithmic character of the curves have slightly inflated values. As a result, during comparison with the other alloys both k_p and mass gain per unit surface must be taken under consideration. As it can be seen in the Table 2, the $Zr_{43}Cu_{45}Al_{12}$ alloy compares favorably with the $Zr_{50}Cu_{43}Al_7$, within the whole considered temperature range (Ref 18), with lower mass gains per unit surface and smaller long-term k_p values, confirming that an increase of Al content at the cost of Zr increases the oxidation resistance. In the case of $Zr_{47.5}Cu_{47.5}Al_5$ (Ref 17) and $Zr_{36}Cu_{58}Al_6$ (Ref 16) alloys the situation is not as clear, suggesting that Al content exclusively is not the only factor determining oxidation resistance as both these alloys in some of the temperatures showed lower mass gains and k_p. The others factors that seem to play a role are proportions between Cu and Zr as well as method of alloy preparation.

The logarithmic character of the kinetic has not been reported for the Cu-Zr-Al-based BMGs (Ref 12, 15-18, 20, 21). In general, such type of kinetic is considered to occur mostly in low and intermediate temperatures, generally below 300-400 °C (Ref 22, 23). While in the case of parabolic relations, most of the models is based on the Wagner model of diffusion-controlled kinetics (Ref 24), the logarithmic relations in oxidation processes can be derived basing on multiple different processes, with most of them being extremely complex, often leading to semi-empirical equations. Mott in his work (Ref 25) derived the logarithmic relations for the case, where the work required to bring an electron from the metal into the oxide is higher than the work required to bring a positive ion from the metal to an interstitial position in the oxide. Basing on this assumption, he concluded that for very thin films (<20 Å) the electrons will pass through the oxide layer by a quantum mechanical tunnel effect in such rate, that the process will be controlled by the diffusion of metal ions leading to parabolic relation. However for the case of thicker layers (30-40 Å), the tunnel effect will be limiting factor leading to relation:

$$x = x_0 \ln\left(\frac{K}{x_0} t + \text{const}\right), \quad \text{(Eq 3)}$$

where K and x_0 are the constants (with the x_0 being temperature independent) and x is the layer thickness, making Eq 3 essentially the same as Eq 1. After the logarithmic stage, Mott assumed that the rate of growth must be determined by the thermionic emission of electrons followed by their diffusion, leading to a slow parabolic growth.

Fromhold in his series of articles (Ref 26-30) discussed in details processes which could lead to the logarithmic kinetics. The main mechanism proposed by him was an electron flow controlled by space charge in oxide film. However, these models were also limited to the thicknesses of up to 1000 Å. Probably the most interesting explanation of logarithmic kinetics for our case, is the one presented by Uhlig (Ref 31). In his work, he assumed that if oxide and metal have different electron affinities, one of the materials will lose its electrons on the expense of the second one. This process will lead to a creation of space charge, which compensate for the difference in affinities. In the case of the oxides, the excess charge associates itself mainly at the lattice imperfections. Due to their restricted number, the space charge may extend into the oxide film even for several thousands of angstroms. Although the mechanisms differs significantly from the ones presented by Mott and Fromhold, nonetheless the kinetics governing equation also in this case takes a form similar to the one presented in Eq 1:

Table 2 Comparison of the k_p (k_p unit: $g^2/cm^4/s$) and mass gains (MG) per unit surface (MG unit: $\mu g/cm^2$) of different Zr-Cu-Al-based amorphous alloys after 12 h of oxidation

	400 °C	450 °C	500 °C
$Zr_{47.5}Cu_{47.5}Al_5$ [17]			
k_p	5.07×10^{-12}	2.81×10^{-12}	9.89×10^{-13}
MG	274	490	690
$Zr_{36}Cu_{58}Al_6$(a) [16]			
k_p	...	...	...
MG	736	1059(b)	226
$Zr_{50}Cu_{43}Al_7$ [18]			
k_p	7.58×10^{-11}	2.27×10^{-11}	1.46×10^{-12}
MG	2090	2430	669
$Zr_{45}Cu_{43}Al_{12}$			
k_p	1.41×10^{-11}	2.42×10^{-12}	2.41×10^{-12}
MG	1353	636	570

(a) Values given for 10 h of oxidation
(b) Value for temperature of 460 °C

$$x = k_0 ln\left(\frac{1}{\tau} + 1\right), \quad \text{(Eq 4)}$$

with the values of k_0 and τ being temperature-dependent constants. The maximum thicknesses predicted by this model are in order of tens of thousands of Angstroms, making it the closest to the thicknesses recorded during our experiments. Behavior similar to the one proposed by Uhlig had been observed for example during oxidation of copper in temperatures 350-550 °C (Ref 32), where the thickness of the oxide layer after which the logarithmic kinetics transformed to the parabolic one was estimated to be about 10^5 Å.

The currently presented results are rather unique in the light of the most common logarithmic oxidation models, as the thicknesses of the scales are in our case higher than 3.5 μm—an order bigger than even in the case of Uhlig's model. Also, the experimental temperatures should be considered rather high for such type of kinetics. It should however be noted, that most of the theoretical models describe only specific, simplified cases and that the complexity of our system unable their straightforward applications. For the moment, the character of the kinetics can only signalize, that the space charge effects may have a significant influence on the oxidation process in this particular system.

3.3 Microstructure and Phase Constitution

The oxidized samples were examined with RTG and SEM (with EDS detector) methods. The RTG measurements were conducted using both low-angle GID (information about structure near the top of the scale's surface) and standard Bragg-Brentano geometry (information about the bulk of the scale). After that, a cross-section of each of the samples were prepared, using standard Struers procedure and examined using SEM microscopy method. Each distinguishable layer within the scales was examined by EDS method, which while cannot be treated as a quantitative method, allowed to obtain additional information about trends in composition, which could be later combined with RTG results.

A backscattered-electron image (BEI) of the cross-section of the $Zr_{43}Cu_{45}Al_{12}$ BMG oxidized for 12 h at 400 °C is presented in Fig. 4(a) with the corresponding XRD and EDS analysis. As it can be seen, the outer surface of the scale was completely planar, with no cracks visible. The substrate-oxide surface on the other hand, was highly irregular. The two layers in the scale can be clearly distinguished. It should be noted, that thorough whole considered temperature range, the scales exhibited outstanding adhesion to the material. The thickness of the scale was determined to be 11.38 ± 0.5 μm. The XRD analysis revealed presence of tetragonal $ZrO_2(t)$ with minor additions of monoclinic $ZrO_2(m)$, CuO, Cu_2O, and α-Al_2O_3 in the outer portion of the scale. The Cu_2O is not visible closer to the oxide-substrate interface. The simultaneous presence of both tetragonal (normally stable in temperature range 1200-1500 °C) and monoclinic zirconia is typical for oxidized Zr-Cu-based metallic glasses. This is due to the very small size of grains, which stabilizes the high temperature stable tetragonal phase (Ref 15, 17, 18).

A backscattered-electron image (BEI) of the cross-section of the $Zr_{43}Cu_{45}Al_{12}$ BMG oxidized for 12 h in 450 °C is presented in Fig. 4(b) with the corresponding XRD and EDS analysis. Again the outer surface of the scale was completely planar, with no cracks visible. The substrate-oxide surface was much more regular than in the previous case. At least two layers in the scale could be distinguished, with strongly marked transitional area between them (marked with number 2 in Fig. 4). The thickness of the scale was determined to be 4.01 ± 0.25 μm. Basing on the low-angle XRD analysis, the outer portion of the scale consisted mainly of tetragonal zirconia ZrO_2(t) with relatively higher contents of ZrO_2(m), CuO, and Cu_2O than in the sample oxidized in 400 °C. Also, a very weak peak from Al_2O_3 was observed. The inner portion of the scale had a similar composition, however the presence of CuO was not as strongly marked while multiple additional peaks from $ZrO_2(m)$ were observed. It should be noted, that presence of Al_2O_3 correlates with the change of oxidation kinetics character, from parabolic to logarithmic.

Another BEI image of the cross-section of the $Zr_{43}Cu_{45}Al_{12}$ BMG oxidized for 12 h at 500 °C is presented in Fig. 4(c) with the corresponding data. Like in the previous cases, the outer surface of the scale was completely planar, with no cracks visible. The substrate-oxide surface had the most planar shape in this case. Three layers within the scale are visible, with metallic sublayer (Zr depleted) formed on the outer surface of the amorphous substrate. The thickness of the scale was determined to be 3.62 ± 0.25 μm. The outer portion of the scale consisted of $ZrO_2(t)$, with minor addition of CuO and α-Al_2O_3. The inner portion consisted mostly of $ZrO_2(t)$ and $ZrO_2(m)$, with minor addition of CuO, and α-Al_2O_3. Based on the XRD results, the content of α-Al_2O_3 is higher than in the case of the sample oxidized in 450 °C, what can also be correlated with further decrease of oxidation rate.

3.4 Short-Term Oxidation

For the most complicated case (oxidation in 500 °C), a short-term oxidation tests were carried out to determine the time sequence of phase formation. The samples were oxidized for 5, 20, and 60 min and examined using XRD method (Bragg-Brentano geometry). The results are presented in Fig. 5. With the results obtained after 12 h given for comparison. It is

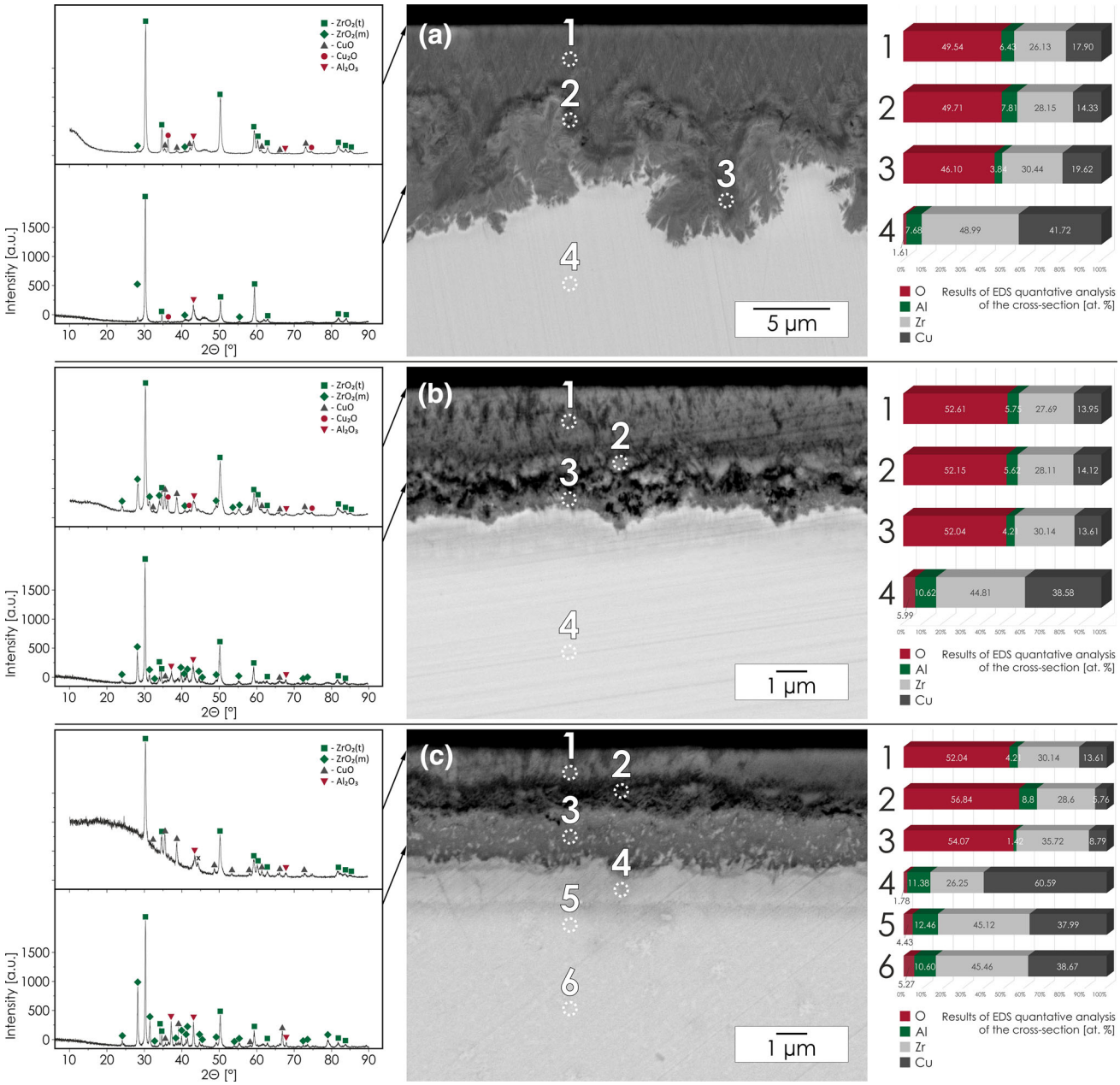

Fig. 4 Cross-sectional BEI micrographs with corresponding XRD spectra and EDS analysis of the $Zr_{43}Cu_{45}Al_{12}$ BMG oxidized for: (a) 12 h in 400 °C, (b) 12 h in 450 °C, (c) 12 h in 500 °C. It should be noted that the EDS results should be treated only qualitatively, especially in the case of oxygen due to limitations of the method (Color figure online)

clear, that the first phase formed is the $ZrO_2(t)$, what is in good agreement with behavior reported for $Zr_{50}Cu_{43}Al_7$ and $Zr_{47.5}Cu_{47.5}Al_5$ (Ref 17, 18). However, the XRD results also revealed the simultaneous formation of α-Al_2O_3 during the earliest stages of oxidation, what in the case of $Zr_{50}Cu_{43}Al_7$ was reported only for times higher than 30 min. This phenomenon can be directly correlated with the difference in the kinetics of oxidation. The logarithmic character of the oxidation kinetics is conditioned by the kinetics during the first 20 min of the process, what can be clearly seen in Fig. 2. The presence of α-Al_2O_3 during this period is the main difference in comparison to the BMGs with lower content of Al. What is more, the content of α-Al_2O_3 grows rapidly within the first 30 min of oxidation, but then somehow slows down, with the kinetics of the other oxides being faster. This suggests that the unexpected behavior of $Zr_{43}Cu_{45}Al_{12}$ results mainly from the early formation α-Al_2O_3. Formation of the $ZrO_2(t)$ and α-Al_2O_3 is followed by nucleation of CuO and $ZrO_2(m)$ what is to be expected. Resulting sequence of oxide formation is different than in the case of $Zr_{50}Cu_{43}Al_7$, where formation of α-Al_2O_3 was preceded by formation of $ZrO_2(t)$ followed by CuO and $ZrO_2(m)$. What deserves further attention is the fact, that no reflexes which could be attributed to the formation of metallic Zr-depleted sublayer formed beneath the scale were observed, what was the case for both $Zr_{50}Cu_{43}Al_7$ and $Zr_{47.5}Cu_{47.5}Al_5$. The early formation of α-Al_2O_3 indicates, that this oxide plays significant role in the oxidation kinetics of the system thorough whole duration of the process.

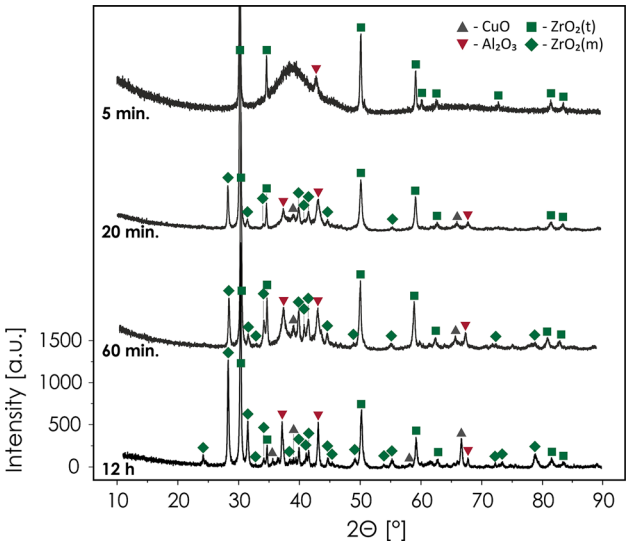

Fig. 5 XRD spectra of the $Zr_{43}Cu_{45}Al_{10}$ BMG oxidized in 500 °C for various times

4. Conclusions

The oxidation behavior of the $Zr_{43}Cu_{45}Al_{12}$ BMG differs significantly from the one reported for $Zr_{50}Cu_{43}Al_7$ and $Zr_{47.5}Cu_{47.5}Al_5$ but also from the ones reported for other Cu-Zr-Al-based BMGs. The α-Al_2O_3 oxide is observed through the whole investigated temperature range, what is supported by both XRD and EDS results. As expected, the oxidation kinetics is in general slower than in the case of glasses with lower Al content, what is especially visible for the temperature of 450 °C, where the mass gain is four times lower than the one reported for $Zr_{50}Cu_{43}Al_7$. Thus, combined with the fact that the scale exhibits excellent adhesion to the material beneath with no cracks which could be attributed to the thermal stresses being observed, make the $Zr_{43}Cu_{45}Al_{12}$ alloy better suited to work in elevated temperatures. The main difference in terms of oxidation behavior is, however, the logarithmic character of oxidation kinetics, previously not reported for Zr-Cu glasses. While the origins of logarithmic kinetics can vary, basing on the theoretical models it can be assumed, that such character of kinetics in our case may be a result of presence of space charge. This may suggest that the Al_2O_3, which is most likely responsible for the kinetics inversion, may be forming a thin, continuous layer, altering the parabolic kinetics.

Acknowledgments

This work is supported by a National Science Center, Poland decision No. DEC-2011/02/A/ST8/00280.

References

1. T. Zhang, A. Inoue, and T. Masumoto, Amorphous Zr-Al-TM (TM = Co, Ni, Cu) Alloys with Significant Supercooled Liquid Region of Over 100 K, *Mater. Trans. JIM*, 1991, **32**, p 1005–1010
2. A. Inoue, Stabilization of Metallic Supercooled Liquid and Bulk Amorphous Alloys, *Acta Mater.*, 2000, **48**, p 279–306
3. D. Wang, H. Tan, and Y. Li, Multiple Maxima of GFA in Three Adjacent Eutectics in Zr-Cu-Al Alloy System: A Metallographic Way to Pinpoint the Best Glass Forming Alloys, *Acta Mater.*, 2005, **53**, p 2969–2979
4. N. Mattern, J. Bednarcik, M. Stoica, and J. Eckert, Temperature Dependence of the Short-Range Order of $Cu_{65}Zr_{35}$ Metallic Glass, *Intermetallics*, 2013, **32**, p 51–56
5. A. Ishii, A. Iwase, Y. Fukumoto, Y. Yokoyama, T. Konno, and F. Hori, Effect of Thermal Annealing on the Local Structure in ZrCuAl Bulk Metallic Glass, *J. Alloys Compd.*, 2010, **504**, p S230–S233
6. Q. Wang, J. Qiang, Y. Wang, J. Xia, X. Zhang, and C. Dong, Formation and Optimization of Cu-Based Cu-Zr-Al Bulk Metallic Glasses, *Mater. Sci. Forum*, 2005, **475-479**, p 3381–3384
7. A. Inoue and T. Zhang, Fabrication of Bulk Glassy $Zr_{55}Al_{10}Ni_5Cu_{30}$ Alloy of 30 mm in Diameter by a Suction Casting Method, *Mater. Trans. JIM*, 1996, **37**, p 185–187
8. D. Kawase, A.P. Tsai, A. Inoue, and T. Masumoto, Crystallization on Supercooled Liquid in Metallic Zr-Cu-Al Glasses, *Appl. Phys. Lett.*, 1993, **62**, p 137
9. A.I. Salimon, M.F. Ashby, Y. Brechet, and A.L. Greer, Bulk Metallic Glasses: What Are They Good For?, *Mater. Sci. Eng. A*, 2004, **375-377**, p 385–388
10. L. Xia, K.C. Chan, L. Liu, and G. Wang, Glass Forming Ability and Mechanical Properties of $Zr_{50}Cu_{42}Al_8$ Bulk Metallic Glass, *J. Phys. D Appl. Phys.*, 2008, **41**, p 225410
11. H. Men, X.K. Wang, J.Y. Fu, C.L. Ma, and T. Zhang, Formation and Mechanical Properties of Cu-Zr-Al-Sn Bulk Metallic Glasses, *Mater. Trans. JIM*, 2006, **47**, p 194–197
12. K. Mondal, U.K. Chatterjee, and B.S. Murty, Oxidation Behavior of Multicomponent Zr-Based Amorphous Alloys, *J. Alloys Compd.*, 2007, **433**, p 162–170
13. L. Jastrow, U. Köster, and M. Meuris, Catastrophic Oxidation of Zr-TM (Noble Metals) Glasses, *Mater. Sci. Eng. A*, 2004, **375-377**, p 440–443
14. M. Kilo, M. Hund, G. Suer, A. Baiker, and A. Wokaun, Reaction Induced Surface Segregation in Amorphous CuZr, NiZr and PdZr Alloys: An XPS and SIMS Depth Profiling Study, *J. Alloys Compd.*, 1996, **236**, p 137–150
15. W. Kai, H.H. Hsieh, T.G. Nieh, and Y. Kawamura, Oxidation behavior of a Zr-Cu-Al-Ni amorphous alloy in air at 300-425 °C, *Intermetallics*, 2002, **10**, p 1265–1270
16. C.Y. Tam, C.H. Shek, and W.H. Wang, Oxidation Behavior of a Cu-Zr-Al Bulk Metallic Glass, *Rev. Adv. Mater. Sci.*, 2008, **18**, p 107–111
17. W. Kai, T.H. Ho, H.H. Hsieh, Y.R. Chen, D.C. Qiao, F. Jiang, G. Fan, and P.K. Liaw, Oxidation Behavior of CuZr-Based Glassy Alloys at 400 °C to 500 °C in Dry Air, *Metall. Mater. Trans. A*, 2007, **39**, p 1838–1846
18. W. Kai, P.C. Lin, W.S. Chen, C.P. Chuang, P.K. Liaw, H.H. Huang, and H.H. Hsieh, Air-Oxidation of a $Zr_{50}Cu_{43}Al_7$ Bulk Metallic Glass at 400-500 °C, *Corros. Sci.*, 2012, **64**, p 98–104
19. T.A.M. Aboki, M.L. Masse, A. Dezellus, P. Ochin, and R. Portier, First Investigations on Twin-Rolled $Zr_{59}Cu_{20}Al_{10}Ni_8Ti_3$ Bulk Amorphous Alloy by Mechanical Spectroscopy, *Mater. Sci. Eng. A*, 2004, **370**, p 330–335
20. L. Liu and K.C. Chan, Oxidation of $Zr_{55}Cu_{30}Al_{10}Ni_5$ Bulk Metallic Glass in the Glassy State and the Supercooled Liquid State, *Appl. Phys. A*, 2005, **80**, p 1737–1744
21. W. Kai, F. Renm, P.C. Kao, R.F. Wang, C. Chuang, M.W. Freels, and P.K. Liaw, Air-Oxidation of a $Cu_{45}Zr_{45}Al_5Ag_5$ Bulk Metallic Glass, *Adv. Eng. Mater.*, 2009, **11**, p 380–386
22. S. Mrowec, *An Introduction to the Theory of Metal Oxidation*, National Bureau of Standards and the National Science Foundation, Washington, D.C., 1982
23. P. Kofstad, *High Temperature Corrosion*, Elsevier Applied Sciences, London, 1988

24. C. Wagner, Beitrag zur Theorie des Anlaufvorgangs, *Z. Phys. Chem. B*, 1933, **21**, p 25–41
25. N.F. Mott, The Theory of the Formation of Protective Oxide Films on Metals II, *Trans. Faraday Soc.*, 1940, **35**, p 472–483
26. A.T. Fromhold, Space Charge in Growing Oxide Films, *J. Chem. Phys.*, 1963, **38**, p 282–283
27. A.T. Fromhold, Space Charge in Growing Oxide Films. II. Nonhomogeneous field, *J. Chem. Phys.*, 1963, **38**, p 2041–2043
28. A.T. Fromhold, Space Charge in Growing Oxide Films. III. Multispecies Diffusion, *J. Chem. Phys.*, 1963, **39**, p 2278–2282
29. A.T. Fromhold, Space Charge in Growing Oxide Films. IV. Rate Effects Deduced by an Averaging Technique, *J. Chem. Phys.*, 1964, **40**, p 3335–3343
30. A.T. Fromhold, Space Charge in Growing Oxide Films. V. Perturbation Coefficients and Second-Order Treatment, *J. Chem. Phys.*, 1966, **44**, p 1628–1636
31. H.H. Uhlig, Initial Oxidation Rate of Metals and the Logarithmic Equation, *Acta Metall.*, 1956, **4**, p 541–554
32. R.F. Tylecote, The Oxidation of Copper at 350 °C-900 °C in Air, *J. Inst. Met.*, 1950, **78**, p 327–350